Journal of Power Sources 405 (2018) 45–50

Contents lists available at ScienceDirect

Journal of Power Sources

journal homepage: www.elsevier.com/locate/jpowsour

Conformal coating of cobalt oxide on solid oxide fuel cell cathode and resultant continuously increased oxygen reduction reaction kinetics upon operation

Yun Chen[a,*], Alec Hinerman[a], Liang Liang[a], Kirk Gerdes[b], Sergio Paredes Navia[a], Jacky Prucz[a], Xueyan Song[a]

[a] Department of Mechanical & Aerospace Engineering, West Virginia University, Morgantown, WV, 26506, USA
[b] U.S. DOE, National Energy Technology Laboratory, Morgantown, WV, 26507, USA

HIGHLIGHTS

- Conformal CoO_x layer is deposited on LSM/YSZ backbone of SOFC cathode using ALD.
- CoO_x ALD layer continuously improves the oxygen reduction reaction upon operation.
- CoO_x ALD layer interacts with the backbone and formed catalytic $Co_{0.7}Mn_{0.3}O_x$.
- $Co_{0.7}Mn_{0.3}O_x$ exhibits Bi-model distribution on LSM and YSZ surfaces.

ARTICLE INFO

Keywords:
Solid oxide fuel cell
Atomic layer deposition
Cobalt oxide
Oxygen reduction reaction

ABSTRACT

To improve the sluggish oxygen reduction reaction from the cathode of solid oxide fuel cells (SOFCs), a conformal layer of catalytic CoO_x grains was deposited onto the internal surface of LSM/YSZ composite cathode of commercial cells, through atomic layer deposition (ALD). Upon the electrochemical operation, the ALD coated cell has dramatic reduction of the polarization resistance, and the power density exhibits continuous increase over the course of 172 h operation at 750 °C and reaches the cell performance enhancement by a factor of 1.6, in comparison with that from the baseline operated for 96 h. Such performance enhancement was attributed to the combination of the newly added triple phase boundaries for promoting the oxygen reduction reaction, as well as the accelerated oxygen transport on the cathode surface. The present work opens the further research direction for ALD coating of non-precious metal catalyst to boost the performance of as-fabricated SOFCs.

1. Introduction

Rising technologies such as fuel cells generate electricity without producing environmentally damaging pollutants. Solid oxide fuel cells (SOFCs) [1] are advantageous over other types of fuel cells owning to their high electrical efficiency and versatility of fuel choice, including hydrocarbons [2]. Currently, there are intense worldwide efforts to improve the SOFC performance, including lowering the SOFC operating temperature to increase the cell durability, and lower the fabrication and operation cost of SOFC stacks and entire plant [3]. However upon operating at lower temperatures (750 °C or lower), resistances from key components intensify. To the most part, reduction of oxygen at the cathode is thermally activated, requires high activation energy, and exhibits slow reaction kinetics at lower temperatures. Sluggish reactions at the cathode thus contribute to a significant portion of the overall energy losses of the SOFC. Currently, the development of material systems with high catalytic activity for oxygen reduction reaction (ORR) [4] proves to be essential in improving the performance of SOFCs.

The state-of-the-art catalyst for ORR in the cathode of SOFC are complex perovskite oxides including $(La_{1-x}Sr_x)MnO_3$ (LSM), $(La_{1-x}Sr_x)(Co_{1-y}Fe_y)O_3$ (LSCF), and $(La_{1-x}Sr_x)CoO_3$ (LSC) [5]. Among those electro-catalysts, LSM has excellent stability and thermal and chemical compatibilities with yttria stabilized zirconia (YSZ) ionic conductor, and provides electronic conductivity and electrochemical activity for oxygen reduction. However, the performance of LSM based cathodes are inferior to those from LSCF and LSC, due to the lack of the ionic conductivity and the lack of catalytic reactions sites that are limited to

* Corresponding author.
E-mail address: yun.chen@mail.wvu.edu (Y. Chen).

https://doi.org/10.1016/j.jpowsour.2018.10.022
Received 2 August 2018; Received in revised form 6 October 2018; Accepted 8 October 2018
Available online 13 October 2018
0378-7753/

the length of the triple phase boundaries (TPBs). The performance of the LSM cathode is thus often limited by its low oxygen ion conductivity at reduced temperatures, which diminishes the effective length of the TPBs or the number of the active sites for the ORR.

With the current technology for manufacture of SOFC using those well-developed complex oxide starting to mature, it would be obviously critical if the additional exotic catalyst could be engineered onto the internal surface of LSM/YSZ to improve the performance of cathodes by infiltration, while still maintaining the advantageous properties of LSM/YSZ backbone [6]. Among the various materials for infiltration, the CoO_x was considered to be promising catalyst for ORR [7,8]. However, the effect of CoO_x infiltration on the SOFC performance are reported to be controversial [9,10]. While the CoO_x has been reported to enhance the performance of LSM/YSZ cathodes [11], there are also evidence showing the addition of CoO_x had a negligible effect on both the *V-I* curve and the impedance spectrum. For the thin film $La_{0.6}Sr_{0.4}CoO_{3-\delta}$, performance degradation was even observed upon coating Co_3O_4 by atomic layer deposition (ALD) [12–14]. In addition to those controversial reports, it is believed that the activity of Co_3O_4 nanoparticles are subjected to fast coarsening at elevated temperatures, thus diminishing the activity quickly. To suppress the coarsening, the infiltration composite consisting of CeO_2 and $SrCrO_3$ were developed to prevent the Co_3O_4 [15].

In comparison with solution based infiltration and other thin film depositions such as pulsed laser deposition, ALD vapor could easily penetrate into the active layer of the cathode that is usually at least 50 microns underneath the cathode exterior surface. Most importantly, ALD could render the formation of conformal and uniform layer of catalyst onto the internal surface of porous cathode that is with complex 3D topography [16–19]. Here we demonstrate the effect of ALD coating of conformal CoO_x layer onto the internal surface of LSM/YSZ cathode of commercial cells. Upon the electrochemical operation, the ALD coated cell has dramatic reduction of the polarization resistance. In the meanwhile, the cell power density exhibits continuous increase over the course of 172 h operation at 750 °C and achieves cell performance enhancement by a factor of 1.6, in comparison with that from baseline operated for 96 h. The physical and nanostructure origin of the SOFC performance enhancement was systematically explored using the combination of electrochemical impedance spectroscopy, the corresponding impedance spectra deconvolution, and post-operation nanostructure imaging and chemistry analysis.

2. Experimental section

Commercially available, anode supported solid oxide button cells fabricated by Materials and Systems Research, Inc. (MSRI, Salt Lake City, UT) were employed for the experiments described in the current study. MSRI cells are composed of five layers as follows, starting from the anode: ~0.9 mm thick Ni/YSZ cermet layer which supports the cell structure; 15 μm thick Ni/YSZ active layer; ~12 μm thick YSZ electrolyte; ~15 μm thick $La_{0.8}Sr_{0.2}MnO_3$ (LSM)/YSZ active layer; and 50 μm thick, pure LSM current collecting layer. The cell active area (limited by the cathode) is 2 cm^2. The exposure area of the anode to fuel is about 3.5 cm^2. Total 2 cells from the same batch of the commercial cells were subsequently processed and studied.

The ALD process was performed on a GEMStar ALD system equipped with an ozone generator (Pacific Ozone Technology). The Bis (cyclopentadienyl)cobalt (II), min. 98% (Cobaltocene) (Strem Chemicals, Inc), and ozone were used as Co precursor and oxidant, respectively. During the processing of growing a CoO_x layer, the sample stage was firstly preheated to 275 °C and then total 250 ALD cycles were performed to build up a 10 nm CoO_x layer. During the ALD processing, no specific treatment or masking was applied on the NiO/YSZ anode.

The infiltrated button cell along with one baseline cell were tested on a test stand at 750 °C. The hydrogen and air stream flow rates were controlled separately using two mass flow controllers. During the operation, a 600 mL/min air flow rate and a 600 mL/min fuel flow rate were used. Both samples were loaded at a constant current density of 0.3 A/cm^2 for desired periods. The cell performance was examined using the test stand integrated TrueData-LOAD system and the impedance spectra was collected between 0.05 Hz and 100 kHz using a potentiostat/galvanostat (Solartron 1287) equipped with a frequency response analyzer (Solartron 1260) periodically for comparison.

The ALD infiltrated cell were sectioned and subjected to nanostructural examination using high resolution (HR) Transmission Electron Microscopy (TEM). All the TEM examinations were conducted in the cathode active layer. TEM samples were prepared by mechanical polishing and ion milling in a liquid nitrogen cooled holder. Electron diffraction, diffraction contrast and HRTEM imaging were performed using a JEM-2100 operated at 200 kV. Chemical analysis was carried out under TEM using energy dispersive X-ray Spectroscopy (EDS).

3. Results

3.1. Enhancement of cell power density, reduction of resistance and implication of two distinct catholic polarization processes

The power density of the baseline Cell #1 and the CoO_x coated Cell #2 and their resistance changes upon electrochemical operation are briefed in Table 1. Fig. 1 shows the performance of the Cell #1 at 24 h and the coated Cell #2 at various operating times. In comparison with the baseline cell, power density at 24 h for the Cell #2 was observed at 0.48 W/cm^2 at 0.8 V and a factor of 1.4 higher than that of the Cell #1. The Cell #2 shows continuously increased performance as operating at constant current of 0.3 A/cm^2 during the 172 h and achieved cell performance enhancement by a factor of 1.6, in comparison with the baseline Cell #1 operated for 96 h. To our knowledge, this is by far the largest performance enhancement that was achieved for commercial cells using solution based infiltration and ALD coating of non-precious metals.

Fig. 2a shows the Nyquist plot of the Cell #1 at 0 h, 24 h and 96 h. R_s and R_p for the baseline cell were measured at 0.054 Ω cm^2 and 0.566 Ω cm^2 after 24 h operation, respectively. Fig. 2b shows the Nyquist plot of Cell #2. R_s value of 0.066 Ω cm^2 at 24 h from the cell #2 is actually higher than that of Cell #1 and R_s from Cell #2 has little change during the operation up to for 172 h. On the other hand, R_p of

Table 1
Electrochemical performance of the baseline and the CoO_x infiltrated cells operated for various times.

Cells	Operating time (h)	Ohmic resistance R_s (Ω cm^2)	Polarization Resistance R_p (Ω cm^2)	Current density i at 0.8 V (A/cm^2)	Power density P at 0.8 V (A/cm^2)	Peak power density (A/cm^2)
Baseline	0	0.043	0.641	0.372	0.298	0.423
#1	24	0.046	0.576	0.421	0.337	0.526
	96	0.047	0.546	0.431	0.345	0.558
10 nm	0	0.07	0.492	0.540	0.430	0.669
CoO_x	24	0.06	0.457	0.606	0.480	0.766
Layer	102	0.06	0.401	0.670	0.531	0.836
#2	172	0.06	0.392	0.693	0.550	0.873

Table 2
Chemistry of different local regions indicated by circled numbers in Fig. 5.

EDS spot	O	Mn	Co	La	Sr	Zr	Y	Normalized Approximate Formula
1	68.41	10.76	20.83	–	–	–	–	$Co_{0.7}Mn_{0.3}O_x$
2	68.28	10.51	21.21	–	–	–	–	$Co_{0.7}Mn_{0.3}O_x$
3	69.11	10.85	20.04	–	–	–	–	$Co_{0.7}Mn_{0.3}O_x$
4	69.53	13.76	2.33	12.23	2.16	–	–	$(La_{0.8}Sr_{0.2})_{0.9}(Mn_{0.9}Co_{0.1})O_x$
5	66.20	16.43	1.05	13.06	3.26	–	–	$(La_{0.8}Sr_{0.2})_{0.9}(Mn_{0.9}Co_{0.1})O_x$
6	58.62	15.11	26.27	–	–	–	–	$Co_{0.6}Mn_{0.4}O_x$
7	49.80	2.56	–	1.22	–	38.83	7.59	–
8	55.58	1.61	–	1.19	–	35.37	6.25	–

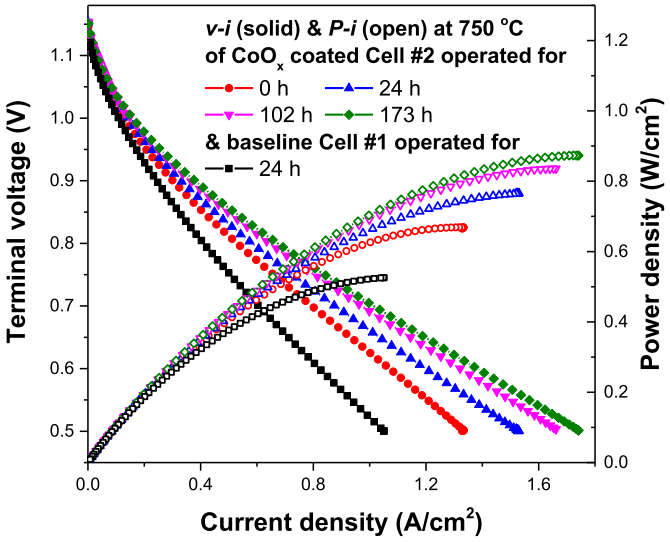

Fig. 1. Polarization curves of the baseline Cell#1 and the Cell#2 coated with CoO_x operated for various times.

the infiltrated cell was measured at 0.452 Ω cm^2 at 24 h and significantly lower than the baseline Cell#1. Indeed, the Impedance spectroscopy reveals that the higher performance of the Cell #2 is due to the much lower non-ohmic impedance. Bode plots were obtained intermittently during the cell operations for Cell #1 and Cell #2. As shown in Fig. 3a and Fig. 3b, the dominant change of the impedance is located in the frequency range between ~1 and ~100 Hz for both the Cell #1 and the ALD coated Cell #2.

Bode plots provide critical clues to identify dominant mechanisms among various cell processes and bode plots of impedance spectra could qualitatively lead to better understand insight of a cell reaction kinetics including the mass and charge transfer and variation of the reaction resistance in the cathode. However, the overlapping of multiple processes makes it difficult to discern the individual polarization processes attributed to various mass transport, and ORR. To better understand the effect of ALD coating CoO_x layer on the ORR processes, the deconvolution [20–22] analysis of was employed to analyze the impedance data in this study. Using deconvolution analysis, the distribution of relaxation times (DRT) resolves the impedance spectrum into a higher resolution plot where individual polarization processes can be identified [20–22]. The detail protocol of the applied deconvolution is introduced in one literature [23]. The deconvolution spectra of the Cell #1 and Cell #2 are present in Fig. 3a and b, respectively. In the spectra, each deconvolution distribution was normalized and multiplied by its respective polarization resistance. Such a data processing allows one to compare between different impedance measurements. In the resulting plot of distribution function g(f) vs log frequency, the area underneath each peak reflected the resistance of a corresponding physical process [23]; therefore, the larger the area under the peak, the higher the resistance of that processes.

The deconvolution spectra in Fig. 3c indicate that, for the baseline Cell #1, one dominant peak is present at ~5 Hz, and another weak higher frequency arc at ~12.5 Hz becomes a barely visible shoulder due to its overlap with the neighboring enlarged impedance arc (at ~5 Hz). In general, the physical processes occurring at the characteristic frequencies of 5–150 Hz range could be assigned to cathode activation polarization ORR at TPBs [20,21,24]. Nevertheless, depending on the cell backbone chemistry, the peaks could shift a little bit to either directions under the identical cell operation conditions [20,24,25]. In the baseline Cell #1, the peak 1 (P_1) at frequency range of ~5 Hz continuously decreased when the operation time increased from 0 to 96 h, that is consistent with the literature reports stating that LSM/YSZ cathode experience activation process that having TPB extended during the initial operation of ~70 h [26]. It is known that LSM based cathodes can be activated significantly by the application of a cathodic polarization [27,28]. Such an activation behavior of LSM based cathodes was attributed to the broadening of the TPBs as a result of an

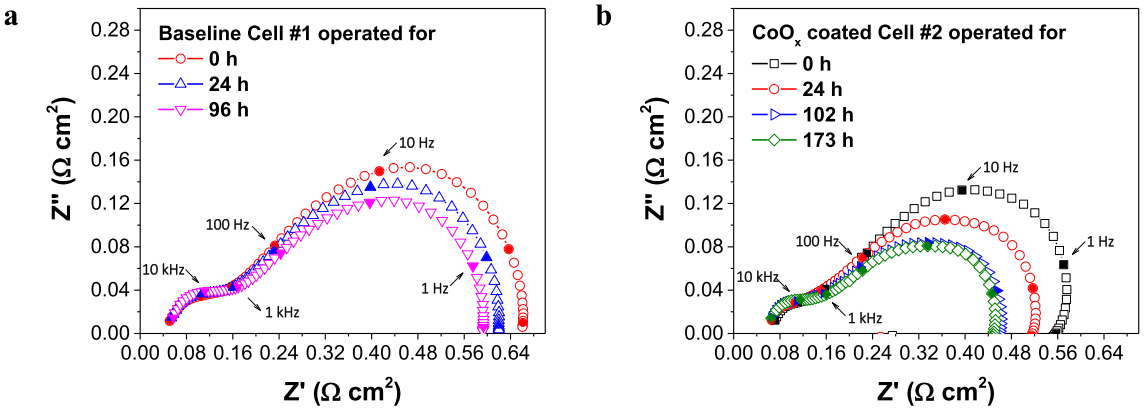

Fig. 2. Nyquist plots of: **a**, the baseline Cell #1, and **b**, the CoO_x coated Cell #2 examined at 0.3 A/cm^2 after operated for various time. The Solid markers indicate the characteristic frequencies in the Nyquist plots.

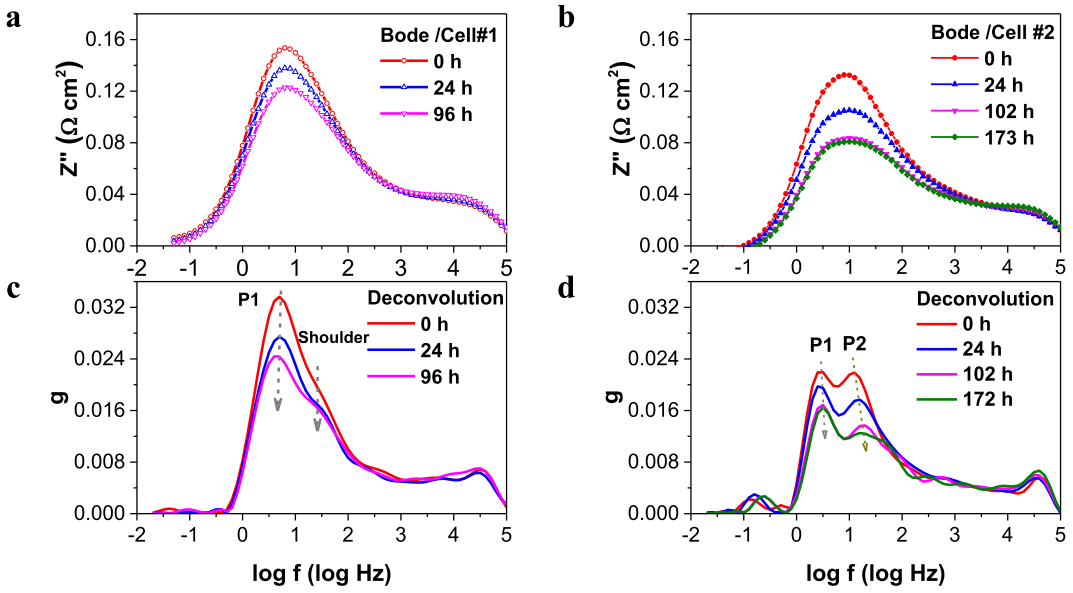

Fig. 3. Bode plots of the baseline Cell#1 and the CoO_x coated Cell #2 are shown in **a** and **b**. The corresponding impedance deconvolution spectra are shown in **c** and **d** in which distribution function g is calculated from experimental impedance data in Figures **a** and **b**. In Figures **c** and **d**, P_1 and P_2 indicate the trend of the peaks at 4–5 Hz and at 12–13 Hz, respectively. The baseline cell does not show an obvious peak at ~12.5 Hz but instead, a shoulder could be seen.

increase in local oxygen vacancy concentration induced by cathodic polarization [29,30]. Meanwhile, the P_1 in the baseline cell almost peaks at the same frequency range of ~5 Hz with the increase of the operation duration indicating the unchanged cathode backbone chemistry towards the cell operation.

By contrast to the Cell #1 that has one dominant peak, Cell #2 exhibit two distinguishable arcs present at ~4–5 Hz (P_1) and at ~13 Hz (P_2) respectively as shown in Fig. 3d, and both arcs present much lower amplitude than that of the Cell #1 operated under the same duration/condition. The presence of the arc at frequency range of ~4 Hz indicates the existence of an extra distinguishable polarization process present in Cell #2. At 0 h operation, both arcs at P_1 and P_2 have similar g values implying two corresponding cathodic processes with similar impact to the entire cathode function. In comparison with that of the Cell #1, both arcs for Cell #2 significantly decrease their amplitude upon increase of the operation time, and the P_2 experienced faster drop with the increase of the operation duration to about 172 h. The peak of P_2 at frequency in the range of 5–150 Hz could be attributed to cathode activation polarization at TPBs [20–23].

It is also worthwhile to mention that, remarkably different from the Cell # 1 that has arc P_1 peaking almost at the same frequency range, both arcs in Cell #2 continuously shift slightly to the higher frequency range with the increase of the operation indicating a continuous change of the chemistry of cathode backbone upon cell operation.

Apparently, ALD coating of a CoO_x layer on the surface of LSM/YSZ cathode has changed the cathode reaction pathways and introduced two different cathodic polarization that may involves two distinct processes for each has its dissociative oxygen adsorption and transport of oxygen species to the TPBs.

3.2. Bi-model nanostructure evolution of CoOx layer on LSM/YSZ backbone surface

TEM images in Fig. 4a shows the conformal coating of the as-deposited CoO_x layer on both the LSM and the YSZ backbone surface. The as-deposited layer appears to be dense and very uniform with the thickness of ~10 nm (in Fig. 4b). The as-deposited state of CoO_x is also crystallized with the plate-shaped nanograins of ~15 nm elongated along the surface of the LSM/YSZ backbone.

After 172 h operation, the Cell #2 is subjected to nanostructure

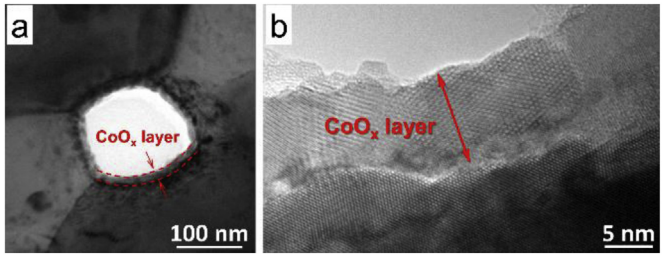

Fig. 4. TEM images show the conformal coating of the as-deposited CoO_x layer on the internal surface LSM/YSZ cathode. **a**, LSM/YSZ backbone surface is covered with a uniform coating layer. **b**, The 10 nm as-deposited state of CoO_x is crystallized with the plate-shaped nano-grains of ~15 nm elongated along the backbone surface.

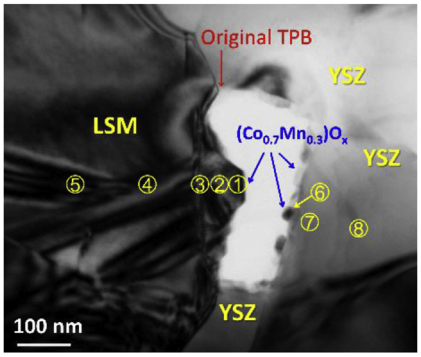

Fig. 5. TEM images show the nanostructure of the CoO_x coating layer after operation for 172 h. The EDS examination were conducted for those numbered spots and the results are listed in Table 2. The size of the circles indicates approximate beam size being used for EDS spectrum collection.

imaging and chemistry analysis under TEM and the results are shown in Fig. 5 and Table 2. One distinct structure feature shows that the CoO_x ALD layer interact strongly with the backbone, but experiences different morphology on LSM and YSZ surface. For those on the LSM grain surface, the CoO_x layer develops into large island shaped grains with the dimension of ~100 nm (in Fig. 5). Furthermore, there is significant

cation inter-diffusion between the CoO_x layer and LSM backbone, leading to the product with typical chemistry of close to $(Co_{0.7}Mn_{0.3})O_x$ nanograins (EDS spots 1, 2 and 3 in Fig. 5 and Table 2). On the other hand, the LSM phase becomes Co doped LSM, showing the gradient of Co concentration decreasing from the original LSM grain surface into the LSM grain interior. The typical chemistry of the near LSM grain surface that is just underneath the secondary phase $(Co_{0.7}Mn_{0.3})O_x$ grains is $(La_{0.8}Sr_{0.2})_{0.9}(Mn_{0.9}Co_{0.1})O_x$ (EDS spot 4 in Fig. 5 and Table 2). And it gradually changes to LSM grains with Mn:Co ratio of 94:6 from the grain interior that is ~200 nm away (spot 5 in Fig. 5 and Table 2) from the LSM grain original surface. In other words, the cation inter-diffusion between Mn and Co has caused Co concentration gradient that continuously decreases from the grain surface to the grain interior. Such diffusion driven chemistry change must have occurred during the cell operation at 750 °C and should probably continuously take place upon further cell operation.

By contrast to the big island shaped $Co_{0.7}Mn_{0.3}O_x$ grains on the LSM surface, for those deposited on the YSZ backbone surface, the initial 10 nm continuous coating layer was developed into discrete Mn doped CoO_x grains. Such Mn doped CoO_x grains are single-layered and plate shaped and exhibit much smaller grains in the size of ~15 nm in height and ~20 nm long. Their population is large and the distance between the neighboring grains are typical much less than ~50 nm. EDS examination indicates the Mn doped CoO_x grains on the YSZ surface is in chemical formula of close to $Co_{0.7}Mn_{0.3}O_x$ (spot 6 in Fig. 5) and remains to be the same as that on the LSM surface. However, Co cation does not incorporate into the backbone YSZ grains as indicated by EDS spots 7 and 8 in Table 2. Minor amount of La is shown in EDS analysis of the YSZ grains. La presents in the bulk YSZ of LSM/YSZ cathode even in the as-received cell and La-concentration in YSZ keeps constant upon cell operation. EDS study shows Mn presents in the YSZ grains with slightly higher amount (of spot 7) near the YSZ grain surface and lower amount (of spot 8) far into the YSZ grain interior. This observation is supported by the literature reports [31] indicating that Mn diffusion from LSM to YSZ during the cell fabrication, and Mn saturated in YSZ. The very limit of Mn concentration in YSZ phase implies Mn in the $Co_{0.7}Mn_{0.3}O_x$ grains on the YSZ surface is from the LSM grains through surface diffusion.

Such bi-model distribution of the $Co_{0.7}Mn_{0.3}O_x$ grains on the LSM/YSZ backbone is schematized in Fig. 6. The bi-model distribution of $Co_{0.7}Mn_{0.3}O_x$ grains is probably caused by the different diffusion pathways, while the $Co_{0.7}Mn_{0.3}O_x$ on LSM surface is from the LSM underneath and grown into large crystal grains. The grain growth is both parallel and perpendicular to the backbone LSM grain surface. By contrast, the $Co_{0.7}Mn_{0.3}O_x$ on YSZ surface is associated with the cation Mn surface diffusion and resulted in the single layered $Co_{0.7}Mn_{0.3}O_x$ grains with constant height of ~10 nm and same as that of the as-deposited CoO_x layer.

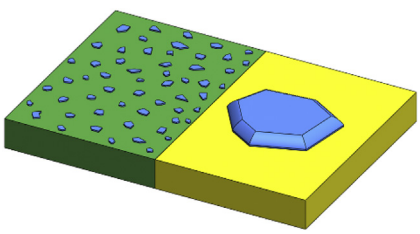

Fig. 6. Schematic of bi-model distribution of $Co_{0.7}Mn_{0.3}O_x$ (in blue color) on the backbone YSZ (in green color) and backbone LSM (in yellow color). (For interpretation of the references to color in this figure legend, the reader is referred to the Web version of this article.)

4. Discussion

4.1. Impact of $Co_{0.7}Mn_{0.3}O_x$ layer at TPB and YSZ surface on the cathode performance

After operation at 750 °C, the continuous decreased polarization resistance R_p indicates the as-deposited CoO_x layer appears to develop interaction with the LSM/YSZ backbone that favors the electrochemical reactions. As shown in Fig. 5, at the original TPB region, the $Co_{0.7}Mn_{0.3}O_x$ grains may have formed a bridge linking the LSM/YSZ grains. On the YSZ surface, there are single layered discrete ~10 nm thick $Co_{0.7}Mn_{0.3}O_x$ grains stabilized on the YSZ surface. Even the $Co_{0.7}Mn_{0.3}O_x$ are sometimes discrete and did not form the continuously network, the distance of the neighboring $Co_{0.7}Mn_{0.3}O_x$ grains are less than ~50 nm, where the effective TPBs could be extended to through polarization [32]. As the intrinsic electro-catalytic $Co_{0.7}Mn_{0.3}O_x$ nanograins bridging the LSM/YSZ grains and sitting on the ionic conducting YSZ substrate, it will dramatically increase the oxygen absorption and dissociation, the oxygen ions thus could quickly transport away along the $Co_{0.7}Mn_{0.3}O_x$/YSZ interface. The existence of such high density $Co_{0.7}Mn_{0.3}O_x$ nanograins thus increased the electrochemical reactions sites and lowered the R_p.

4.2. Impact of CoO_x coating on performance of LSM

The cell performance improvement induced by ALD coating of CoO_x could also be attributed to the enhancement of surface processes on the LSM phase itself. For the $Co_{0.7}Mn_{0.3}O_x$ grains sitting on the LSM grain surface, in the thin film structures, there are continuous evidence showing that the interface [33] between the oxides such as LSM/$Co_{0.7}Mn_{0.3}O_x$ could possess substantial ionic conductivity thus create additional pathways for oxygen transport and extend TPB length. It is not clear how the results from ALD layer of the present study could be directly related to the thin film studies yet. However, the enhanced ionic conductivity at LSM/$Co_{0.7}Mn_{0.3}O_x$ interface could be possibly one of the causes of the performance enhancement.

Furthermore, during the operation, the LSM grain becomes $(La_{0.8}Sr_{0.2})_{0.9}(Mn_{0.8}Co_{0.2})O_x$ in the surface layer of LSM backbone. The studies reported the interfacial polarization resistances of a Co doped LSM cathode are smaller than those of an LSM cathode at 600-800 °C [26]. The performance of a cell based on a Co doped LSM cathode is ~34% higher than that based on an LSM cathode while maintaining comparable long-term stability, indicating that Co doped LSM is a promising cathode material for SOFCs. There is also evidence showing that the amount of Co in $La_{0.8}Sr_{0.2}Mn_{1-x}Co_xO_3$ perovskites which results in the maximum oxygen transport is 25% [26].

4.3. Correlation between the impedance and nanostructure

Nanostructure analysis clearly indicate that for the ALD coated SOFC cell, besides the original TPBs, both the LSM and YSZ grain surface carries additional TPBs for the ORR and the mass and charge transfer for the electrochemical reactions. It is obvious that multiple factors contribute simultaneously to the reduced resistance and improved cell performance. Such nanostructure analysis is supported with the impedance and related impedance spectra deconvolution showing that the two corresponding cathodic processes with similar impact to the entire cathode function. Upon the further cell operation, the performance increase and the resulting cation inter-diffusion will eventually saturate to reach equilibrium for both the LSM grain and $Co_{0.7}Mn_{0.3}O_x$ grains on the LSM/YSZ backbone. Co doped LSM are reported to be remarkable stable for long term operation. Most importantly, the present study demonstrates the stable $Co_{0.7}Mn_{0.3}O_x$ nanograins upon the long-term operation. The cause of the formation of the stable $Co_{0.7}Mn_{0.3}O_x$ nanograins are currently unclear. The electrochemical operation and the related mass charge transfer along the

interfaces and grain boundaries, and the reduced oxygen partial pressure in the cathode during the SOFC operation all could have contributed significantly to the formation of such stable nanograins. The current results certainly warrant the further study in this regard.

5. Conclusions

ALD coating a layer of CoO_x on the internal backbone of LSM/YSZ cathode largely decreases the non-ohmic resistance, and thus the power density exhibits continuous increase over the course of 172 h operation at 750 °C and achieved cell performance enhancement by a factor of 1.6. Impedance analysis shows the CoO_x coated cathode depicts two distinguishable polarization processes that contribute almost equally to the mass and charge transfer and ORR. The CoO_x layer interacts with the backbone through cation inter-diffusion and exhibit bi-model distribution of the bigger $Co_{0.7}Mn_{0.3}O_x$ grains on LSM surface and remarkably stable $Co_{0.7}Mn_{0.3}O_x$ nanograins of ~10 nm on the YSZ surface. The reduction of polarization resistance was attributed to the combination of the newly added TPB sites and expanded TPBs for promoting the ORR, as well as the enhanced oxygen transport on the cathode surface. The present work opens the further research direction for ALD coating of non-precious metal catalyst to boost the performance of as-fabricated SOFCs.

Acknowledgements

X. Song, A. Hinerman, L. Liang and S. Paredes Navia acknowledge the financial support from DE-FE0023386, DE-FE0031251. X. Song acknowledges the support from NSF-DMR 1254594.

References

[1] L. Yang, S.Z. Wang, K. Blinn, M.F. Liu, Z. Liu, Z. Cheng, M.L. Liu, Science 326 (2009) 126–129.
[2] S. Park, R. Craciun, J.M. Vohs, R.J. Gorte, Direct oxidation of hydrocarbons in a solid oxide fuel cell: I. Methane oxidation, J. Electrochem. Soc. 146 (10) (1999) 3603–3605.
[3] E.D. Wachsman, K.T. Lee, Lowering the temperature of solid oxide fuel cells, Science 334 (6058) (2011) 935–939.
[4] Y. Chen, W. Zhou, D. Ding, M. Liu, F. Ciucci, M. Tade, Z. Shao, Advances in cathode materials for solid oxide fuel cells: complex oxides without alkaline earth metal elements, Adv. Energy Mater. 5 (18) (2015) 1500537.
[5] Subhash C. Singhal, Kevin Kendall, High-temperature Solid Oxide Fuel Cells: Fundamentals, Design, and Applications, Elsevier Advanced Technology, New York, 2003.
[6] D. Ding, X. Li, S.Y. Lai, K. Gerdes, M. Liu, Enhancing SOFC cathode performance by surface modification through infiltration, Energy Environ. Sci. 7 (2) (2014) 552–575.
[7] D. Chen, C. Huang, R. Ran, H.J. Park, C. Kwak, Z. Shao, New Ba0.5Sr0.5Co0.8Fe0.2O3 − δ + Co3O4 composite electrode for IT-SOFCs with improved electrical conductivity and catalytic activity, Electrochem. Commun. 13 (2) (2011) 197–199.
[8] Z. Zhang, J. Wang, Y. Chen, S. Tan, Z. Shao, D. Chen, In situ formation of a 3D core-shell and triple-conducting oxygen reduction reaction electrode for proton-conducting SOFCs, J. Power Sources 385 (2018) 76–83.
[9] Y. Huang, J.M. Vohs, R.J. Gorte, An examination of LSM-LSCo mixtures for use in SOFC cathodes, J. Electrochem. Soc. 153 (6) (2006) A951–A955.
[10] Y. Ren, Y. Cheng, R.J. Gorte, K. Huang, Toward stabilizing Co3O4 nanoparticles as an oxygen reduction reaction catalyst for intermediate-temperature SOFCs, J. Electrochem. Soc. 164 (10) (2017) F3001–F3007.
[11] K. Yamahara, C.P. Jacobson, S.J. Visco, X.-F. Zhang, L.C. De Jonghe, Thin film SOFCs with cobalt-infiltrated cathodes, Solid State Ionics 176 (3–4) (2005) 275–279.
[12] B.J. O'Neill, D.H. Jackson, J. Lee, C. Canlas, P.C. Stair, C.L. Marshall, J.W. Elam, T.F. Kuech, J.A. Dumesic, G.W. Huber, Catalyst design with atomic layer deposition, ACS Catal. 5 (3) (2015) 1804–1825.
[13] E. Mutoro, E.J. Crumlin, M.D. Biegalski, H.M. Christen, Y. Shao-Horn, Enhanced oxygen reduction activity on surface-decorated perovskite thin films for solid oxide fuel cells, Energy Environ. Sci. 4 (9) (2011) 3689–3696.
[14] H.J. Choi, K. Bae, D.Y. Jang, J.W. Kim, J.H. Shim, Performance degradation of lanthanum strontium cobaltite after surface modification, J. Electrochem. Soc. 162 (6) (2015) F622–F626.
[15] Y. Ren, Y. Cheng, R.J. Gorte, K. Huang, Toward stabilizing Co3O4 nanoparticles as an oxygen reduction reaction catalyst for intermediate-temperature SOFCs, J. Electrochem. Soc. 164 (10) (2017) F3001–F3007.
[16] T.M. Onn, M. Monai, S. Dai, L. Arroyo-Ramirez, S. Zhang, X. Pan, G.W. Graham, P. Fornasiero, R.J. Gorte, High-surface-area, iron-oxide films prepared by atomic layer deposition on γ-Al2O3, Appl. Catal. Gen. 534 (2017) 70–77.
[17] T.M. Onn, S. Zhang, L. Arroyo-Ramirez, Y. Xia, C. Wang, X. Pan, G.W. Graham, R.J. Gorte, High-surface-area ceria prepared by ALD on Al2O3 support, Appl. Catal. B Environ. 201 (2017) 430–437.
[18] M. Rahmanipour, Y. Cheng, T.M. Onn, A. Donazzi, J.M. Vohs, R.J. Gorte, Modification of LSF-YSZ composite cathodes by atomic layer deposition, J. Electrochem. Soc. 164 (7) (2017) F879–F884.
[19] Y. Chen, K. Gerdes, X. Song, Nanoionics and nanocatalysts: conformal mesoporous surface scaffold for cathode of solid oxide fuel cells, Sci. Rep. 6 (2016) 32997.
[20] A. Leonide, V. Sonn, A. Weber, E. Ivers-Tiffée, Evaluation and modeling of the cell resistance in anode-supported solid oxide fuel cells, J. Electrochem. Soc. 155 (1) (2008) B36–B41.
[21] A. Leonide, B. Ruger, A. Weber, W.A. Meulenberg, E. Ivers-Tiffee, Impedance study of alternative (La,Sr)FeO3-δ and (La,Sr)(Co,Fe)O3-δ MIEC cathode compositions, J. Electrochem. Soc. 157 (2) (2010) B234–B239.
[22] H. Schichlein, A.C. Müller, M. Voigts, A. Krügel, E. Ivers-Tiffée, Deconvolution of electrochemical impedance spectra for the identification of electrode reaction mechanisms in solid oxide fuel cells, J. Appl. Electrochem. 32 (8) (2002) 875–882.
[23] H. Finklea, X. Chen, K. Gerdes, S. Pakalapati, I. Celik, Analysis of SOFCs using reference electrodes, J. Electrochem. Soc. 160 (9) (2013) F1055–F1066.
[24] B. Liu, H. Muroyama, T. Matsui, K. Tomida, T. Kabata, K. Eguchi, Analysis of impedance spectra for segmented-in-series tubular solid oxide fuel cells, J. Electrochem. Soc. 157 (12) (2010) B1858–B1864.
[25] M. Kornely, A. Neumann, N.H. Menzler, A. Leonide, A. Weber, E. Ivers-Tiffee, Degradation of anode supported cell (ASC) performance by Cr-poisoning, J. Power Sources 196 (17) (2011) 7203–7208.
[26] Y. Bai, M. Liu, D. Ding, K. Blinn, W. Qin, J. Liu, M. Liu, Electrical and electrocatalytic properties of a La0.8Sr0.2Co0.17Mn0.83O3 − δ cathode for intermediate-temperature solid oxide fuel cells, J. Power Sources 205 (2012) 80–85.
[27] M.J. Jørgensen, S. Primdahl, C. Bagger, M. Mogensen, Effect of sintering temperature on microstructure and performance of LSM–YSZ composite cathodes, Solid State Ionics 139 (1–2) (2001) 1–11.
[28] M.J. Jørgensen, M. Mogensen, Impedance of solid oxide fuel cell LSM/YSZ composite cathodes, J. Electrochem. Soc. 148 (5) (2001) A433–A442.
[29] A. Barbucci, R. Bozzo, G. Cerisola, P. Costamagna, Characterisation of composite SOFC cathodes using electrochemical impedance spectroscopy. Analysis of Pt/YSZ and LSM/YSZ electrodes, Electrochim. Acta 47 (13–14) (2002) 2183–2188.
[30] E.P. Murray, S. Barnett, (La, Sr) MnO3–(Ce, Gd) O2 − x composite cathodes for solid oxide fuel cells, Solid State Ionics 143 (3–4) (2001) 265–273.
[31] M. Backhaus-Ricoult, K. Adib, T.S. Clair, B. Luerssen, L. Gregoratti, A. Barinov, In-situ study of operating SOFC LSM/YSZ cathodes under polarization by photoelectron microscopy, Solid State Ionics 179 (21–26) (2008) 891–895.
[32] S.B. Adler, Factors governing oxygen reduction in solid oxide fuel cell cathodes, Chem. Rev. 104 (10) (2004) 4791–4843.
[33] S. Lee, J.L. MacManus-Driscoll, Research Update: fast and tunable nanoionics in vertically aligned nanostructured films, Apl. Mater. 5 (4) (2017) 042304.